scientific reports

Check for updates

OPEN

A trial deep learning-based model for four-class histologic classification of colonic tumor from narrow band imaging

Takeshi Shimizu[1], Yoshihiro Sasaki[2]✉, Kei Ito[1], Masashi Matsuzaka[2], Hirotake Sakuraba[3] & Shinsaku Fukuda[4]

Narrow band imaging (NBI) has been extensively utilized as a diagnostic tool for colorectal neoplastic lesions. This study aimed to develop a trial deep learning (DL) based four-class classification model for low-grade dysplasia (LGD); high-grade dysplasia or mucosal carcinoma (HGD); superficially invasive submucosal carcinoma (SMs) and deeply invasive submucosal carcinomas (SMd) and evaluate its potential as a diagnostic tool. We collected a total of 1,390 NBI images as the dataset, including 53 LGD, 120 HGD, 20 SMs and 17 SMd. A total of 598,801 patches were trimmed from the lesion and background. A patch-based classification model was built by employing a residual convolutional neural network (CNN) and validated by three-fold cross-validation. The patch-based validation accuracy was 0.876, 0.957, 0.907 and 0.929 in LGD, HGD, SMs and SMd, respectively. The image-level classification algorithm was derived from the patch-based mapping across the entire image domain, attaining accuracies of 0.983, 0.990, 0.964, and 0.992 in LGD, HGD, SMs, and SMd, respectively. Our CNN-based model demonstrated high performance for categorizing the histological grade of dysplasia as well as the depth of invasion in routine colonoscopy, suggesting a potential diagnostic tool with minimal human inputs.

Although it is relatively simple for human observers to recognize and describe the visual elements in empirical terms, it has been remarkably difficult to accurately define and analyze them with a computer. The electronic endoscope has allowed us to quantify any element making up a digitized endoscopic image through mathematical processes. Several studies have evaluated the effectiveness of feature extraction for computer-aided diagnosis (CAD) to classify the endoscopic severity of ulcerative colitis[1,2] and to assess the risk of developing gastric cancer among Helicobacter pylori-positive patients[3]. However, the diagnostic accuracy of feature engineering was limited due to the challenges in extracting features for image analysis in gastrointestinal diseases.

With the proliferation of CNN, the task of classifying objects in natural images can be solved simply by presenting examples of images and the names of the objects to a neural network that acquired all its knowledge from the training data[4]. This groundbreaking technology has freed engineers from feature engineering and endoscopists from knowledge-based image interpretation. The CNN-based supervised learning has been applied in the automated localization of gastric cancer in routine gastroscopies[5] and the automated detection of colon polyps[6]. Several studies have reported the utilization of a CNN-based model for distinguishing adenomatous from non-adenomatous polyps[7], adenomatous from hyperplastic diminutive colorectal polyps [8], and neoplastic polyps from non-neoplastic polyps [9]. The fine-tuning of a pre-trained CNN for gastric precancerous disease classification[10] or the efficient channel attention deep dense CNN for the classification of esophageal disease[11] has also been reported.

However, to the best of our knowledge, a multi-class model for evaluating the grade of histologic dysplasia along with the depth of invasion has not yet been developed. The NBI international colorectal endoscopic (NICE) classification applicable to with or without magnification was proposed for diagnosing submucosal invasive colon

[1]Department of Gastroenterology, Sendai City Medical Center Sendai Open Hospital, 5-22-1 Tsurugaya, Miyagino-ku, Sendai 983-0824, Japan. [2]Department of Medical Informatics, Hirosaki University Hospital, 53 Hon-cho, Hirosaki 036-8563, Japan. [3]Department of Gastroenterology and Hematology, Hirosaki University Graduate School of Medicine, 5 Zaifu-cho, Hirosaki 036-8562, Japan. [4]Department of Community Medical Support, Hirosaki University Graduate School of Medicine, 5 Zaifu-cho, Hirosaki 036-8562, Japan. ✉email: gahiro@hirosaki-u.ac.jp

cancer[12]. However, criteria for classification described in empirical terms[12] may inevitably suffer from a variety of biases in evaluation leading to different accuracy varying with endoscopists and disturb comparison of accuracy among different endoscopist communities. This study aimed to develop a trial CNN-based supervised learning model for evaluating histologic atypism or invading depth from NBI images of detected colonic neoplastic lesions and evaluate the potential as a diagnostic tool.

Methods

Preparation of endoscopic images. NBI images of neoplastic lesions from patients who underwent endoscopic or surgical resection at Sendai City Medical Center Sendai Open Hospital from April 2017 to December 2019 were used for this single center retrospective study. Characteristics of collected NBI images are summarized in Table 1. A total of 1390 NBI images were sampled from a total of 210 lesions with definite histologic diagnosis[13]: 53 low-grade dysplasia (LGD); 120 high grade dysplasia or mucosal carcinoma (HGD); 20 superficially invasive (the depth of the invasive front < 1000 μm) submucosal carcinoma (SMs) and 17 deeply invasive (the depth of the invasive front > 1000 μm) submucosal carcinomas (SMd). Pathological diagnosis was conducted by pathologists unaware of the study design in a blinded manner. The diagnosis of a mucosal lesion, LGD or HGD was assigned to the most severe grade regardless of the size of the component. Sampled picture number per lesion was 5.5 to 7 samples with an averaged image capturing conditions: no magnification 41.0%; low magnification 37.9%; high magnification 21.1%. The images of a solitary lesion at varying magnifications were carefully chosen to minimize potential bias in the selection process. The video endoscopes CF-HQ290ZI, PCF-H290ZI, PCF-H290TI and video endoscopy system EVIS LUCERA ELITE CV-290/CLV-290SL (Olympus Medical Systems, Co., Ltd., Tokyo, Japan) were used.

Preparation of dataset. NBI images (Fig. 1a) were manually partitioned into the lesion (Fig. 1b) and background (Fig. 1c) from which the patch images (128 × 128 pixels) were cropped starting from the left upper corner (white dotted patch), rightwards (white solid patch), then downwards (red solid patch) at every 32-pixel-strides (white and red arrows) over the entire effective region of interest. The patches including blackouts with more than 10% of the effective region were automatically excluded from analysis. Blackouts were defined as regions with the intensity of red component lower than 50. Similarly, the patches with halations exceeding 5% of the effective region were also excluded. Halations were defined as regions with the intensity of green component higher than 250. In this study, the patches were further classified into in-focus patches and out-of-focus ones according to the amount of spatial high frequency area extracted by high pass filter with a cut-off of 6.25% Nyquist frequency. The in-focus patches were classified into (0) background (BG), (1) LGD, (2) HGD, (3) SMs

Histology	Number of lesions	Number of still pictures	Averaged picture number per lesion	Magnification (picture counts/%)		
				None	Low	High
LGD	53	294	5.5	126/42.9	120/40.8	48/16.3
HGD	120	840	7.0	345/41.1	305/36.3	190/22.6
SMs	20	138	6.9	59/42.8	46/33.3	33/23.9
SMd	17	118	6.9	40/33.9	56/47.5	22/18.6
total	210	1390	6.6	570/41.0	527/37.9	293/21.1

Table 1. Collected NBI images for dataset. NBI, narrow band imaging; HGD, high grade dysplasia; LGD, low grade dysplasia; SMs, superficially invasive submucosal carcinoma; SMd, deeply invasive submucosal carcinoma.

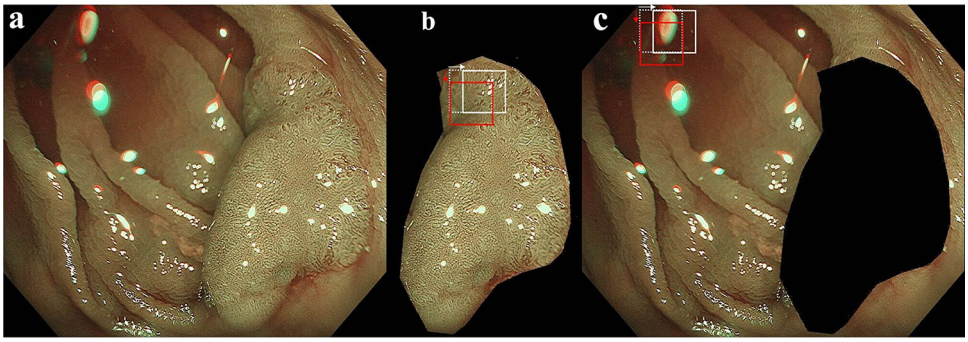

Figure 1. Preparation of dataset. Original NBI image (**a**) were manually partitioned into the lesion (**b**) and background (**c**). The patch images (128 × 128 pixels) were trimmed from the lesion and background starting from the left upper corner (white dotted patch), rightwards (white solid patch), then downwards (red solid patch) at every 32-pixel-strides (white and red arrows) over the entire region of interest.

and (4) SMd, and the out-of-focus ones into (5) background (BG-oof) and 6) lesion (L-oof). A total of 598,801 patches were classified into 7 categories (Table 2). The study did not have any inclusion or exclusion criteria for pictorial quality of the patches by endoscopists. As stated, the patches with excessive blackout or halation were automatically excluded before entry. The study aimed to establish an effective histologic classifier that can be used in any common shooting conditions of NBI.

Evaluation method. We employed cross-validation to obtain more accurate results with less bias in the machine learning studies[14]. In this study, the dataset is randomly partitioned into three equal sized folds, one fold of which is for validation and the other folds are for training. The proportion of labels was equal in each fold. The training and validation processes were repeated three times using different folds each time. The three validation results could then be averaged to produce a single estimation.

Architecture of the CNN. ResNet50 (a CNN) proposed by He et al.[15] and Pytorch were utilized. ResNet50 without pretraining was imported from Pytorch library (torchvision.models). The original patches with 128×128 pixels were converted into images with 224×224 pixels. We tuned hyper parameters, which were set by a human, as follows: optimizer, Adam; loss function, cross entropy loss; number of training epochs, 50; batch size, 256; learning rate, 0.00005 via trial and error; and number of the outer layers, 7 classes.

Image-level classification. An exemplification of SMd and the annotation mask without blackout or halation (denoted by X) are depicted in Fig. 2a,i, respectively. The patches classified into BG, LGD, HGD, SMs, SMd, BG-oof and L-oof, by the trained CNN, are illustrated by white (Fig. 2b), green (Fig. 2c), yellow (Fig. 2d), magenta (Fig. 2e), red (Fig. 2f), dark gray (Fig. 2g) and cyan (Fig. 2h) open squares, respectively, and the corresponding union masks in Fig. 2j–p, respectively. Classification algorithms must be developed by utilizing in-focus patches, without sacrificing pictorial information. Here, the union masks of the patches classified into labels BG, LGD, HGD, SMs and SMd are designated by M0, M1, M2, M3 and M4, respectively. Intersection over union between X and Mi (IoUi) are given by $X \cap Mi / X \cup Mi$ ($i = 0, 1, 2, 3, 4$). The lesion was classified into the argmax among IoUi ($i = 0, 1, 2, 3, 4$), with the IoUi values of 0.12, 0.05, 0.21, 0.04 and 0.57, respectively, leading to label 4 or histologic classification SMd.

Ethics approval and consent to participate. This study was approved by the Committee of Medical Ethics of Hirosaki University Graduate School of Medicine (Aomori, Japan; reference no. 2019–1099) and Sendai City Medical Center (Sendai, Japan: reference no. 2019–0029). Informed consent was obtained in the form of opt-out on our website (https://www.https://www.med.hirosaki-u.ac.jp/hospital/outline/resarch.html), with the

Category	The number of patches
BG	91,571
LGD	52,184
HGD	158,187
SMs	28,049
SMd	20,882
BG-oof	167,081
L-oof	80,847

Table 2. Quantity of clipped patches within each category. BG, background; HGD, high grade dysplasia; LGD, low grade dysplasia; SMs, superficially invasive submucosal carcinoma; SMd, deeply invasive submucosal carcinoma; BG-oof, out-of-focus background; L-oof, out-of-focus lesion.

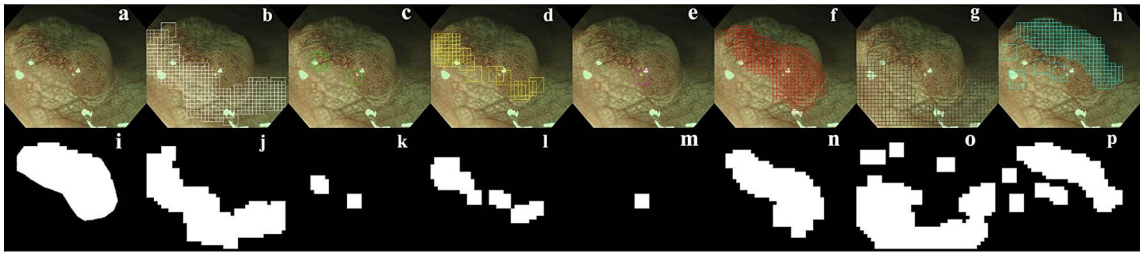

Figure 2. The patch-level histological mapping predicted by the trained model, alongside the annotation mask. An example picture of SMd and the annotation mask without blackout or halation can be seen in (**a**) and (**i**), respectively. White (**b**), green (**c**), yellow (**d**), magenta (**e**), red (**f**), dark gray (**g**), and cyan (**h**) open squares indicate the patches classified as BG, LGD, HGD, SMs, SMd, BG-oof, and L-oof, respectively, with their corresponding union masks visible in (**j–p**), respectively. BG, background; HGD, high grade dysplasia; LGD, low grade dysplasia; SMs, superficially invasive submucosal carcinoma; SMd, deeply invasive submucosal carcinoma; BG-oof, out-of-focus background; L-oof, out-of-focus lesion.

approval of the Committee of Medical Ethics of Hirosaki University Graduate School of Medicine. This study was designed and carried out in accordance with the Declaration of Helsinki.

Results

Accuracy of patch-level and image-level classification. An averaged validation accuracy in the patches with label 0, 1, 2, 3, 4, 5 and 6 was 0.938, 0.876,0.957, 0.907, 0.929, 0.966 and 0.904, respectively (Table3). Table 4 displays the confusion matrix diagram depicting the outcomes of the image-level classification from the patch-based mapping across the entire image area using the trained CNN. The ground truth histology was located on the vertical axis, and the predicted histology was situated on the horizontal axis. Out of 1,390 pictures, 1,371 pictures were correctly classified into the correct histology with a total accuracy of 0.986. The precision and F1-scores were determined to be 0.973, 0.992, 1, 0.967 and 0.978, 0.991, 0.982, 0.980 for LGD, HGD, SMs, and SMd, respectively.

Examples of the patch-based mapping and image-level classification. Figure 3 illustrates the examples of input images, patch-level prediction map and bar graph of IoU. In cases 1, 2, 3 and 4, the ground truth histology was consistent with the predicted histology with the maximum intersection over union. In cases 5 and 6, HGD and SMd were misclassified as SMd and HGD, respectively. In these cases, misclassification of the surrounding background into the true lesion resulted in a lower intersection over union of the true lesion compared to the misclassified ones. A type of misclassification, stemming from an underestimation of the actual lesion compared to misclassified lesions across four SMs, has likely caused a decrease in accuracy relative to other lesions.

Discussion

In this study, we developed a trial CNN-based multi-class histology classifier model for detected colorectal neoplastic lesion in routine colonoscopy still images with NBI mode in common shooting condition. The NBI offers a significant advantage for CNN-based image classification thanks to its ability to provide high contrast or detailed pictorial information without requiring any pre-acquisition preparation. The diagnosis process includes patch-level histology mapping over the entire in-focus region of NBI image, trained on ResNet50 and the calculation of argmax among intersections over union between annotation mask and patch-level union masks for image-level histology. This model achieved an image-level accuracy of 0.986, suggesting its potential as a diagnostic tool.

The advancement of machine learning using CNN has enabled physicians to apply CAD of medical images in their specialized field. The American Society for Gastrointestinal Endoscopy AI Task Force[16] stated that CAD plays a crucial role in screening and surveillance colonoscopy for colorectal cancer prevention. Similarly, a European Society of Gastrointestinal Endoscopy mentioned to the capability of AI for accurately predicting the histology of polyps from endoscopic images and improving the cost-efficiency and safety of colonoscopic

Category	Fold 1			Fold 2			Fold 3			Averaged accuracy
	Total patches	Correct patches	Accuracy	Total patches	Correct patches	Accuracy	Total patches	Correct patches	Accuracy	
BG	30,524	28,634	0.938	30,524	28,625	0.938	30,523	28,637	0.938	0.938
LGD	17,395	15,011	0.863	17,395	15,044	0.865	17,394	15,644	0.899	0.876
HGD	52,729	50,383	0.956	52,729	50,327	0.954	52,729	50,703	0.962	0.957
SMs	9350	8616	0.921	9350	8657	0.926	9349	8163	0.873	0.907
SMd	6961	6115	0.878	6961	6632	0.953	6960	6659	0.957	0.929
BG-oof	55,694	54,108	0.972	55,694	53,855	0.967	55,693	53,386	0.959	0.966
L-oof	26,949	24,664	0.915	26,949	23,758	0.882	26,949	24,695	0.916	0.904

Table 3. Patch-level three-fold validation accuracy. BG, background; HGD, high grade dysplasia; LGD, low grade dysplasia; SMs, superficially invasive submucosal carcinoma; SMd, deeply invasive submucosal carcinoma; BG-oof, out-of-focus background; L-oof, out-of-focus lesion.

Ground truth	Predicted histology				total	Recall
	LGD	HGD	SMs	SMd		
LGD	289	4	0	1	294	0.983
HGD	6	832	0	2	840	0.990
SMs	2	2	133	1	138	0.964
SMd	0	1	0	117	118	0.992

Table 4. Confusion matrix and image-level accuracy. BG, background; HGD, high grade dysplasia; LGD, low grade dysplasia; SMs, superficially invasive submucosal carcinoma; SMd, deeply invasive submucosal carcinoma.

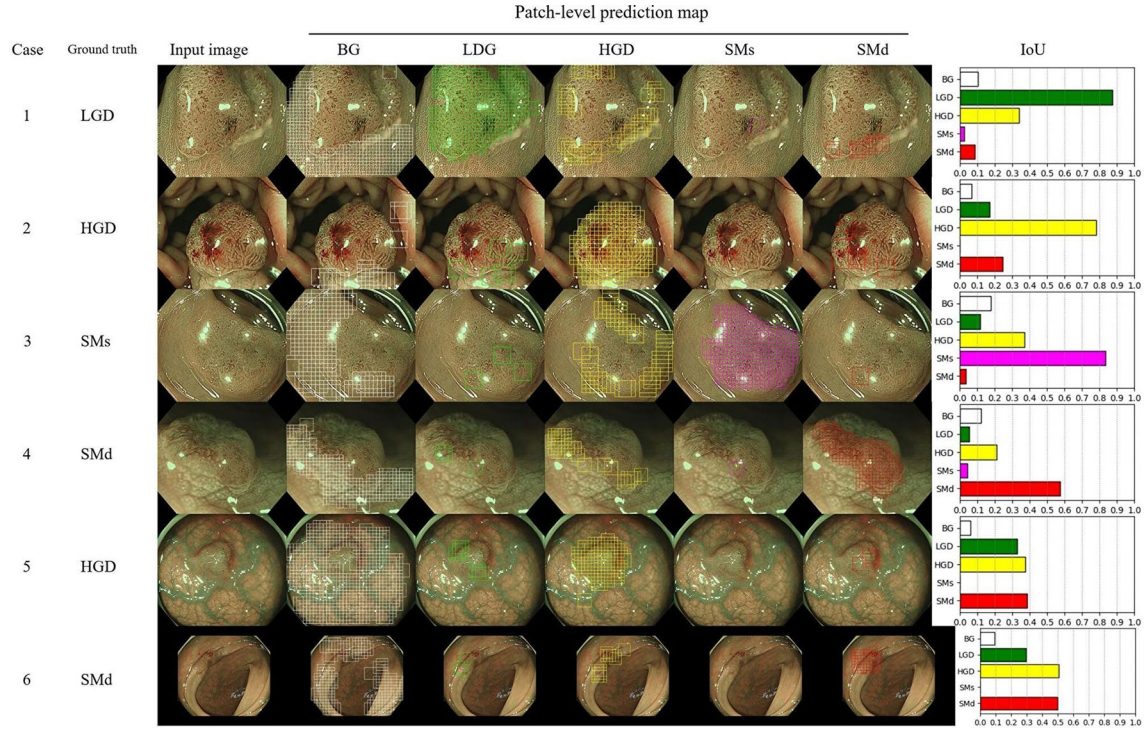

Figure 3. Input images with patch-level prediction map and IoU. BG, background ; HGD, high grade dysplasia ; LGD, low grade dysplasia ; SMs, superficially invasive submucosal carcinoma ; SMd, deeply invasive submucosal carcinoma; IoU, intersection over union.

colorectal cancer screening and surveillance[17]. The supervised learning of a CNN has enabled the development of a model for automated detection of colon polyps[6], as well as binary classification models for distinguishing adenomatous from non-adenomatous polyps (with a ten-fold validation accuracy of 0.751)[7], adenomatous from hyperplastic diminutive colorectal polyps (with an accuracy of 94%)[8], and neoplastic polyps from non-neoplastic polyps (with a high confidence rate of 0.85)[9].

However, a CNN model for multiclass differentiation among low-grade dysplasia, high-grade dysplasia, and carcinoma with superficial or deep submucosal invasion has not been developed. Although invading depth is determinant for therapeutic intervention (endoscopic resection or surgery), it has been evaluated so far by endoscopists with the use of knowledge-based criteria[12,18] which inevitably suffers from a variety of biases in evaluation. One study has reported a CNN-based binary class prediction model for deeply submucosal invasive carcinoma with an overall accuracy of 85.5%, which is comparable to that of expert endoscopists[19]. Although it must be done with caution, comparison of model accuracy between studies with different designs revealed a prediction accuracy of 0.991 for carcinoma with deeply submucosal invasion in this study. To accurately compare the accuracy of ML models regardless of algorithm and class numbers, the promotion of a benchmark data set library with annotation masks[20] is essential.

A patch-based CNN has been utilized for automated detection of a target area within a whole slide image in digital pathology[21,22]. This method has been recently applied for automated severity mapping along the entire colorectum in patients with ulcerative colitis from capsule endoscopy video files[23], as it is considered to have an advantage when the object for classification is composed of topographically varying elements, such as severity or atypism. When reconstructing histologic maps in resected specimens, one often encounters topographic heterogeneity in the grade of dysplasia as well as invading depth. In this study, a single histology or label was assigned to a single lesion image, thus resulting in similar labels across the entire lesion area, which may have impacted the outcomes. None the less, a multi-class classification model developed from a trained patch-level classifier has achieved a high image-level accuracy of over 0.96, which may provide a potential diagnostic tool with minimal human input in routine colonoscopy.

The limitations of the study were: its single-center, retrospective nature, limited dataset size, and lack of external validation; moreover, other classification models including VGGNets, DenseNets and ViT were not explored; the applicability of the model to diagnosis in the subsequent endoscopy system is uncertain.

Data availability

The data generated or analyzed during this study are included in this published article. Some datasets generated and/or analyzed during the current study are not publicly available due to privacy but are available from the corresponding author on reasonable request.

Received: 20 January 2023; Accepted: 6 May 2023
Published online: 09 May 2023

References

1. Sasaki, Y., Hada, R. & Munakata, A. Computer-aided grading system for endoscopic severity in patients with ulcerative colitis. *Dig. Endosc.* **15**, 206–209. https://doi.org/10.1046/j.1443-1661.2003.00246.x (2003).
2. Sasaki, Y., Fukuda, S., Mikami, T. & Hada, R. Endoscopic Quantification of Mucosal Surfaceroughness for grading severity of ulcerative colitis. *Dig. Endosc.* **20**, 2891–2898. https://doi.org/10.1111/j.1443-1661.2008.00778.x (2008).
3. Sasaki, Y. *et al*. Computer-aided estimation for the risk of development of gastric cancer by image processing. In *Artificial Intelligence in Theory and Practice III* 197–204. https://doi.org/10.1007/978-3-642-15286-3_19 (2010).
4. Krizhevsky, A., Sutskever, I. & Hinton, G. E. ImageNet classification with deep convolutional neural networks. *Commun. ACM* **60**, 84–90. https://doi.org/10.1145/3065386 (2017).
5. Hirasawa, T. *et al.* Application of artificial intelligence using a convolutional neural network for detecting gastric cancer in endoscopic images. *Gastric Cancer* **21**, 653–660. https://doi.org/10.1007/s10120-018-0793-2 (2018).
6. Misawa, M. *et al.* Artificial intelligence-assisted polyp detection for colonoscopy: Initial experience. *Gastroenterology* **154**, 2027–2029. https://doi.org/10.1053/j.gastro.2018.04.003 (2018).
7. Komeda, Y. *et al.* Computer-aided diagnosis based on convolutional neural network system for colorectal polyp classification: preliminary experience. *Oncology* **93**, 30–34. https://doi.org/10.1159/000481227 (2017).
8. Byrne, M. F. *et al.* Real-time differentiation of adenomatous and hyperplastic diminutive colorectal polyps during analysis of unaltered videos of standard colonoscopy using a deep learning model. *Gut* **68**, 94–100. https://doi.org/10.1136/gutjnl-2017-314547 (2019).
9. Rodriguez-Diaz, E. *et al.* Real-time artificial intelligence-based histologic classification of colorectal polyps with augmented visualization. *Gastrointest Endosc.* **93**, 662–670. https://doi.org/10.1016/j.gie.2020.09.018 (2021).
10. Liu, X., Wang, C., Bai, J. & Liao, G. Fine-tuning pre-trained convolutional neural networks for gastric precancerous disease classification on magnification narrow-band imaging images. *Neurocomputing* **392**, 253–267. https://doi.org/10.1016/j.neucom.2018.10.100 (2020).
11. Du, W. *et al.* Automatic classification of esophageal disease in gastroscopic images using an efficient channel attention deep dense convolutional neural network. *Biomed. Opt. Express* **12**, 3066–3081. https://doi.org/10.1364/BOE.420935 (2021).
12. Hayashi, N. *et al.* Endoscopic prediction of deep submucosal invasive carcinoma: validation of the narrow-band imaging international colorectal endoscopic (NICE) classification. *Gastrointest Endosc.* **78**, 625–632. https://doi.org/10.1016/j.gie.2013.04.185 (2013).
13. Bosman, F. T. *et al. WHO Classification of Tumors of the Digestive System* 160–165 (IARC Press, 2010).
14. Ojala, M. & Garriga, G. C. Permutation Tests for Studying Classifier Performance. *J. Mach. Learn. Res.* **11**, 1833–1863 (2010).
15. He, K., Zhang, X., Ren, S. & Sun, J. Deep residual learning for image recognition. In *2016 IEEE Conference on Computer Vision and Pattern Recognition*. https://doi.org/10.48550/arXiv.1512.03385 (2016).
16. Berzin, T. M. *et al.* Position statement on priorities for artificial intelligence in GI endoscopy: A report by the ASGE Task Force. *Gastrointest Endosc.* **92**, 951–959. https://doi.org/10.1016/j.gie.2020.06.035 (2020).
17. East, J. E. *et al.* Advanced endoscopic imaging: European Society of Gastrointestinal Endoscopy (ESGE) technology review. *Endoscopy* **48**, 1029–1045. https://doi.org/10.1055/s-0042-118087 (2016).
18. Kobayashi, S. *et al.* Diagnostic yield of the Japan NBI Expert Team (JNET) classification for endoscopic diagnosis of superficial colorectal neoplasms in a large-scale clinical practice database. *United Eur. Gastroenterol J.* **7**, 914–923. https://doi.org/10.1177/2050640619845987 (2019).
19. Lui, T. K. L. *et al.* Endoscopic prediction of deeply submucosal invasive carcinoma with use of artificial intelligence. *Endosc. Int. Open* **7**, E514–E520. https://doi.org/10.1055/a-0849-9548 (2019).
20. Borgli, H. *et al.* HyperKvasir, a comprehensive multi-class image and video dataset for gastrointestinal endoscopy. *Sci. Data* **7**, 283. https://doi.org/10.1038/s41597-020-00622-y (2020).
21. Hou, L., *et al*. Patch-Based Convolutional Neural Network for Whole Slide Tissue Image Classification. In *2016 IEEE Conference on Computer Vision and Pattern Recognition*. 10.48550 /arXiv.1504.07947 (2016).
22. Roy, K., Bani, D., Bhattacharjee, D. & Nasipuri, M. Patch-based system for Classification of Breast Histology images using deep learning. *Comput. Med. Imaging Graph.* **71**, 90–103. https://doi.org/10.1016/j.compmedimag.2018.11.003 (2018).
23. Higuchi, N. *et al.* Automated evaluation of colon capsule endoscopic severity of ulcerative colitis using ResNet50. *PLoS ONE* **17**, e0269728. https://doi.org/10.1371/journal.pone.0269728 (2022).

Acknowledgements

We would like to thank Takashi Sawai, MD, PhD, Department of Pathology, Sendai City Medical Center, Toru Furukawa, MD, PhD, Fumiyoshi Fujishima, MD, PhD, Satoko Sato, MD, PhD, Department of Pathology, Tohoku University School of Medicine, and Miwa Uzuki, MD, PhD, Department of Nursing, Faculty of Medical Science and Welfare, for histologic evaluations.

Author contributions

Y.S. and T.S. contributed to the study conception and design. T.S. and K.I. collected the clinical data and tumor annotation. Y.S. established the prediction model. Y.S. and T.S. wrote the first draft of the manuscript paper. M.M., H.S. and S.F. contributed to the review, and/or critical revision of the manuscript. All authors have approved the final article. Informed consent was obtained in the form of opt-out on our website (https://www.med.hirosaki-u.ac.jp/hospital/outline/resarch.html), with the approval of the Committee of Medical Ethics of Hirosaki University Graduate School of Medicine.

Competing interests

The authors declare no competing interests.

Additional information

Correspondence and requests for materials should be addressed to Y.S.

Reprints and permissions information is available at www.nature.com/reprints.

Terms and Conditions

Springer Nature journal content, brought to you courtesy of Springer Nature Customer Service Center GmbH (“Springer Nature”).
Springer Nature supports a reasonable amount of sharing of research papers by authors, subscribers and authorised users (“Users”), for small-scale personal, non-commercial use provided that all copyright, trade and service marks and other proprietary notices are maintained. By accessing, sharing, receiving or otherwise using the Springer Nature journal content you agree to these terms of use (“Terms”). For these purposes, Springer Nature considers academic use (by researchers and students) to be non-commercial.
These Terms are supplementary and will apply in addition to any applicable website terms and conditions, a relevant site licence or a personal subscription. These Terms will prevail over any conflict or ambiguity with regards to the relevant terms, a site licence or a personal subscription (to the extent of the conflict or ambiguity only). For Creative Commons-licensed articles, the terms of the Creative Commons license used will apply.
We collect and use personal data to provide access to the Springer Nature journal content. We may also use these personal data internally within ResearchGate and Springer Nature and as agreed share it, in an anonymised way, for purposes of tracking, analysis and reporting. We will not otherwise disclose your personal data outside the ResearchGate or the Springer Nature group of companies unless we have your permission as detailed in the Privacy Policy.
While Users may use the Springer Nature journal content for small scale, personal non-commercial use, it is important to note that Users may not:

1. use such content for the purpose of providing other users with access on a regular or large scale basis or as a means to circumvent access control;
2. use such content where to do so would be considered a criminal or statutory offence in any jurisdiction, or gives rise to civil liability, or is otherwise unlawful;
3. falsely or misleadingly imply or suggest endorsement, approval , sponsorship, or association unless explicitly agreed to by Springer Nature in writing;
4. use bots or other automated methods to access the content or redirect messages
5. override any security feature or exclusionary protocol; or
6. share the content in order to create substitute for Springer Nature products or services or a systematic database of Springer Nature journal content.

In line with the restriction against commercial use, Springer Nature does not permit the creation of a product or service that creates revenue, royalties, rent or income from our content or its inclusion as part of a paid for service or for other commercial gain. Springer Nature journal content cannot be used for inter-library loans and librarians may not upload Springer Nature journal content on a large scale into their, or any other, institutional repository.
These terms of use are reviewed regularly and may be amended at any time. Springer Nature is not obligated to publish any information or content on this website and may remove it or features or functionality at our sole discretion, at any time with or without notice. Springer Nature may revoke this licence to you at any time and remove access to any copies of the Springer Nature journal content which have been saved.
To the fullest extent permitted by law, Springer Nature makes no warranties, representations or guarantees to Users, either express or implied with respect to the Springer nature journal content and all parties disclaim and waive any implied warranties or warranties imposed by law, including merchantability or fitness for any particular purpose.
Please note that these rights do not automatically extend to content, data or other material published by Springer Nature that may be licensed from third parties.
If you would like to use or distribute our Springer Nature journal content to a wider audience or on a regular basis or in any other manner not expressly permitted by these Terms, please contact Springer Nature at

onlineservice@springernature.com